Spatial Vision, Vol. 12, No. 2, pp. 187–209 (1999)

Mechanisms for spatial integration in visual detection: a model based on lateral interactions

MARIUS USHER [1], YORAM BONNEH [2], DOV SAGI [2] and MICHAEL HERRMANN [3]

[1] *Department of Psychology, University of Kent, Canterbury, CT2 7NP, UK*
[2] *Department of Neurobiology, The Weizmann Institute of Science, Rehovot 76100, Israel*
[3] *Max-Planck-Institut für Strömungsforschung, Bunsenstraße 10, D-37073 Göttingen, Germany*

Received 1 April 1998; accepted 31 August 1998

Abstract—Recent studies of visual detection show a configuration dependent weak improvement of thresholds with the number of targets, which corresponds to a fourth-root power law. We find this result to be inconsistent with probability summation models, and account for it by a model of 'physiological' integration that is based on excitatory lateral interactions in the visual cortex. The model explains several phenomena which are confirmed by the experimental data, such as the absence of spatial and temporal uncertainty effects, temporal summation curves, and facilitation by a pedestal in 2AFC tasks. The summation exponents are dependent on the strength of the lateral interactions, and on the distance and orientation relationship between the elements.

1. INTRODUCTION

The mechanisms by which visual information is integrated is an important topic of both visual neuroscience and psychophysics research. Local contrast sensitivity depends on spatial context, and exhibits range-dependent excitatory and inhibitory interactions (Polat and Sagi, 1993; Zenger and Sagi, 1996; Adini *et al.*, 1997). Neurophysiological and neuroanatomic studies of the primary visual cortex have revealed an extensive range of horizontal projections that connect cortical cells with similar response properties (Gilbert, 1992; Knierim and Essen, 1992; Malach *et al.*, 1993; Lund *et al.*, 1993). The effect of these connections is complex, and involves both iso-orientation inhibition (Gilbert, 1992; Grinvald *et al.*, 1994) and collinear facilitation (Kapadia *et al.*, 1995; Polat and Norcia, 1996).

In psychophysics, visual integration can be addressed by studying the threshold for detection of compound stimuli, in relation to the detectability of each component (Sachs *et al.*, 1971; Kulikowski *et al.*, 1973; Legge, 1978; Howell and Hess, 1978;

Robson and Graham, 1981). In such studies, the improvement in detection (i.e. the decrease in threshold) for stimuli corresponding to different spatial detection channels was generally lower than expected from linear summation ($1/n$; where n is the number of components), even when the summation of independent noise in each channel ($1/\sqrt{n}$) was taken into account. The data indicate a flatter function, characterized by $n^{-1/q}$, where the exponent q is typically between 3 and 4.5. Therefore, *probability summation* (PS) was proposed as the mechanism responsible for the weak threshold reduction (Sachs *et al.*, 1971; Quick, 1974; Robson and Graham, 1981; Pelli, 1985). Although the various channels do not interact and no actual summation takes place, a small reduction in threshold (corresponding to summation exponents between 3 and 4.5) is expected if the decision is based on maximal activation among all the channels.

1.1. Effects of spatial configuration on contrast detection

The dependency of contrast detection on the spatial configuration of elements (small Gabor patches) within a visual display was recently studied by Bonneh and Sagi (1998a). The main features of spatial configuration that strongly affect the pattern of threshold improvement are collinearity and spatial proximity. The results indicated that a threshold improvement corresponding to exponents $3 < q < 4.5$ is found, only if the elements are proximal and collinear. In absence of such a configuration (e.g. orthogonal or non-proximal elements), the improvement in threshold is weak (almost flat, which corresponds to exponents > 6). Such an effect is demonstrated in Fig. 1, using experimental data previously reported (Bonneh and Sagi, 1998a), averaging across the two observers. In those experiments, fragments of a smooth elliptic arrangement of Gabor patches (ellipse axis $= 4.8 \times 6.24$ deg) which had approximately the same detection threshold in isolation (single patch sensitivity measured along the contour for different positions and orientations), were used to test contrast summation, i.e. improvement in detection threshold with increased number of patches. When the spacing between the elements was fixed to 3 wavelengths of the Gabor (3λ, see the experiment, fixed-spacing curve), the improvement in the detection threshold was almost linear on a log–log scale that corresponded to exponents between 4 and 4.5. However, when the patches were equally-spaced along the ellipse (see the experiment, equal-spacing curve), little improvement was observed with less than 16 patches, and the curves converged only with 45 or more patches (less than 5λ spacing).

These data present a paradox for the probability-summation scheme. If each detector contributes to the decision independently, the pattern of threshold improvement could not depend on the spatial relationship between local elements, since the maximal activation should be identical for independent non-interacting detectors. The data are also inconsistent with a scheme based on local elongated first-stage filters that integrate across multiple patches (Polat and Tyler, 1997), with limited PS assumed for global integration between these filters. Such a scheme is demonstrated in Fig. 1 titled as 'Filter + PS'. Images similar to the experimental stimuli (but

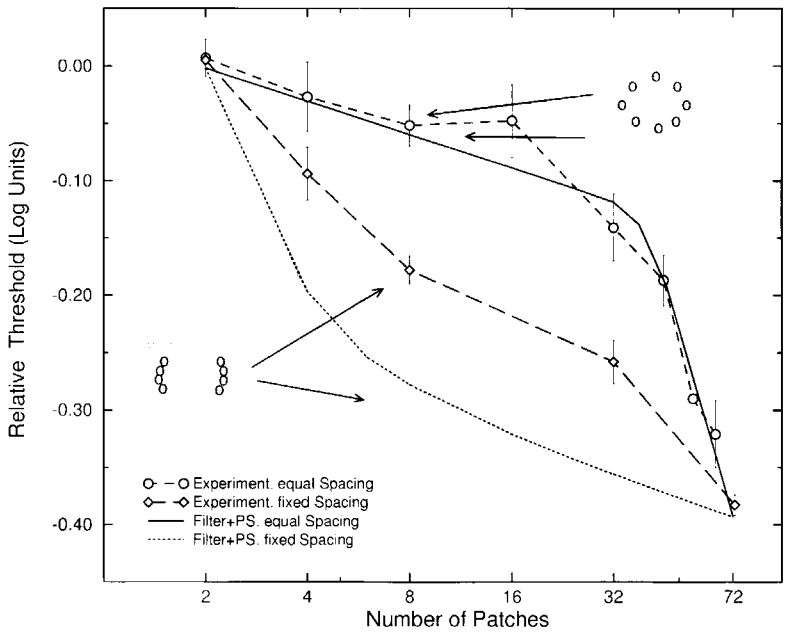

Figure 1. The effect of inter-element distance on the contrast detection threshold for a smooth (collinear) elliptic configuration. Experimental data (the average of two observers from Bonneh and Sagi (1998a)) is compared with a scheme based on elongated first-stage Gabor filters ($\sigma_y/\sigma_x = 2.5$) with a limited probability-summation ($q = 10$). Detection threshold (relative to the threshold of 2 patches) is plotted as a function of the number of patches on a log–log scale for two conditions: *equal spacing* between patches along an elliptic configuration and *fixed spacing* (3λ) along the left and right side fragments of the ellipse. The filtering model matches the equal-spacing curve, but fails to account for the fourth-root summation with the same parameters. The small images demonstrate 8-patch stimulus configurations of the equal (top) and fixed (bottom) spacing conditions.

arranged along a straight line, for simplicity) were convolved (at every pixel) with an elongated Gabor kernel ($\sigma_x = \lambda$, $\sigma_y = r\sigma_x$, r, elongation parameter) followed by a half-wave rectification. A non-linear summation according to the Quick (1974) formula $R = (\sum_i R_i^q)^{1/q}$ (R_i filter responses, q the summation exponent) was then applied (on every pixel R_i) to simulate the experimental power-law (possibly representing probability-summation). The parameters $r = 2.5$ and $q = 11$ were found to fit well the equal-spacing condition, where the proximity limitation is well captured by the locality of the filter. However, using the same parameters, the fixed-spacing curve strongly deviates from the experimental fourth-root summation curve (its first part represents integration within the elongated filter and the rest of the curve is due to the limited PS). This shows that such a scheme cannot generate a uniform power-function in summation experiments, because the RF summation contributes a faster summation slope at small distances. A first-stage filtering scheme is also inconsistent with the phase insensitivity of the effect (Bonneh and Sagi, 1998a), while a similar phase-independent (second-stage) filtering scheme will fail for the same

reasons. However, second-stage mechanisms that continuously integrate along the whole curved contour cannot be rejected.

We conclude that these data suggest that the mechanism responsible for the reduction in threshold is due to interactions between visual channels (see also Bonneh and Sagi, 1998a). Establishment of such a claim, requires demonstration of a scheme for visual integration that is based on lateral interactions and is compatible with the sub-linear pattern of threshold reduction measured in the psychophysical experiments.

1.2. Models based on probability summation

Threshold functions, which are shallow for non-proximal or non-collinear elements (Bonneh and Sagi, 1998a), appear to rule out an exclusive PS scheme. However, one can distinguish between several versions of the PS scheme which may be combined with second-stage filters or lateral-interactions. An essential issue in these models is the locus of variability (noise) in the processing stream (Quick, 1974). Noise may affect each detector independently. A simpler possibility is that noise affects all the detectors in the same way, which could result from either correlated noise or from assuming that the independent noise is much smaller than some global noise that impinges on the system at a later stage. For the latter possibility, probability summation might not be involved in spatial integration of information, but could still play a role in temporal integration (Watson, 1978).

The simplest formulation of the PS scheme is within a high-threshold (HT) model (Sachs *et al.*, 1971; Quick, 1974; Robson and Graham, 1981) where it is assumed that detection occurs when at least one of the detectors passes a threshold. In the HT model, a two alternative forced choice (2AFC) paradigm (choosing one of two frames presented successively, one of which contains the signal and the other of which is empty) is modeled by assuming that the probability for a false detection (FA) is negligible, and that below threshold observers guess. According to this model, and assuming independent noise, the exponent q, which describes the threshold function $\theta(n) \propto n^{-1/q}$, is related to the Weibull exponent in the psychometric function $P(C) = 1 - (1/2)2^{-C^q}$ (C: stimulus contrast). However, experimental evidence for such a relation between the psychometric curve slope and the summation curve exponent is inconclusive. Robson and Graham (1981) found exponents $q \approx 3.5$ for both summation and psychometric curves. However, the values of q estimated from our psychometric curves are close to 6, and strongly depend on the experimental paradigm (q values computed from the staircase data (see *Methods*) are typically around 3). These q values did not depend on the spatial configuration or on the number of elements, and thus, are inconsistent with the summation curve exponents, which vary between 4 and 8.

Another PS model was formulated within the framework of signal-detection (SD) theory (Pelli, 1985; Tyler, 1997b). In this model, false detections are assumed to be relatively high, with subjects performing 2AFC by computing the maximum activation of targets (and noise) in each frame, and then choosing the frame

with a larger maximum. Thus, choice would still be determined by independent registration of the targets (Pelli, 1985), followed by the maximum operation. Such a model was also successfully used by Palmer (Palmer, 1993; Palmer *et al.*, 1993) to explain the effects of set size on contrast increment thresholds in visual search. If uncorrelated noise on the detectors is assumed, the summation curve exponent q will depend on the degree of uncertainty (i.e. the number of channels monitored, which can be greater than the actual number of targets). When the number of monitored channels, M, is not greater than 30 000 as assumed by Pelli (1985) to explain several phenomena (e.g. dipper effects), the q exponents are smaller than 5 (Table 1, in Pelli (1985); see also the Appendix), and do not match the flatter functions ($q > 5$) observed for non-proximal and non-collinear targets.

An alternative SD version of PS assumes that there is no uncertainty, i.e. the number of channels monitored is always equal to the number of targets. This scheme leads to flatter curves ($q > 5$; see Appendix) and thus shows the same tendency as the experimental data for non-collinear and non-proximal elements without uncertainty (Bonneh and Sagi, 1998a) (although the experimental curves are flatter). Accordingly, it leads to a simple prediction: an uncertainty-effect. When observers are uncertain about the location (and number) of targets to be presented at each trial, their performance is expected to deteriorate due to the objective uncertainty in the display (resulting in a shift from the lower to the upper curve in Fig. A.1, in the Appendix).

1.3. Overview of the model

We present a simple computational model, based on standard assumptions about neural processes in the visual cortex and their interaction, to explain the basic pattern of threshold reduction in visual detection tasks. According to our model, each visual element provides direct input to a local detector (a cell-population, presumably in V1) that is activated in proportion to the contrast of the element. The detectors interact by excitatory collinear connections, and detection results from the most active response. A critical feature of such a model is the locus of the variability (noise): local to each detector or global (see Quick, 1974).

In this study, experimental data to constrain the model were obtained by testing the impact of spatial uncertainty on threshold detection. A positive uncertainty effect would support a SD model based on independent noise together with control on monitoring. A negative result would support either a model based on correlated or global noise, or an uncertainty model with very large $M > 30\,000$; in both cases, however, lateral interactions between collinear-detectors are needed to explain the stronger summation found for collinear/proximal elements. We further constrained the model by testing temporal summation and the effect of subthreshold pedestal facilitation.

2. PSYCHOPHYSICS

2.1. Methods

2.1.1. Apparatus. Stimuli were displayed as gray-level modulations on Mitsubishi and Sony color monitors, using a Silicon Graphics Crimson/Reality Engine system. The video format was 60 Hz non-interlaced with 1280×1024 pixels that occupied a 13×10.4 deg area. An 8-bit RGB mode was used, and Gamma correction was applied to produce linear behavior of the displayed luminance. The thresholds for small Gabor signals, that were used here, are high enough (5–40%) to be effectively measured with 8-bit grey-level resolution. The mean display luminance was 40 cd/m^2 in an otherwise dark environment.

2.1.2. Stimuli. Stimuli consisted of displays comprised of multiple Gabor elements. The luminance profile of a single vertical Gabor patch is given by

$$G(x, y) = \cos\left(\frac{2\pi}{\lambda}x + \phi\right)\exp\left(-\frac{x^2 + y^2}{\sigma^2}\right).$$

The Gabor parameters were $\lambda = \sigma = 0.08$ deg of visual angle, which is equivalent to a spatial frequency of 12.5 c/deg with an envelope width of 1.39 cycles at half height, and the phase ϕ was 0. The Gabor patches, whose number varied, were identical in size, and were placed at two opposite sides of a smooth elliptic contour around fixation (ellipse axis $= 4.8 \times 6.24$ deg, inter-element spacing $= 3\lambda$). The single-patch sensitivity along this elliptic contour was previously tested for the same observers, and found to be approximately uniform (Bonneh and Sagi, 1998a) (the aspect ratio was empirically selected to achieve uniform sensitivity). An example of stimuli used is presented in Fig. 2.

2.1.3. Experimental procedures. A 2AFC paradigm was used in all the experiments. Each trial consisted of two stimuli that were being presented sequentially, only one of which had a target (in the 'dipper effect' experiments, both stimuli contained the pedestal). Before each trial, a small fixation circle was presented at the center of the screen. When ready, the observer pressed a key that activated the trial sequence: a no-stimulus interval (0.3 s), a first stimulus presentation, a no-stimulus interval with fixation (1.1 s total, 0.5 s with fixation), and a second stimulus presentation. The duration of stimulus presentation was 117 ms, except for the temporal-summation experiments, where it was varied. The observer was asked to perform a detection task, that is, to determine which of the stimuli contained the target.

Each block consisted of 50 trials (on average), across which the Gabor signal configuration was kept constant, except when positional uncertainty was tested. Screen luminance was kept constant during the trials. The stimuli were viewed binocularly from a distance of 150 cm in a dark environment. Auditory feedback was given by a keyboard bell immediately after an erroneous response.

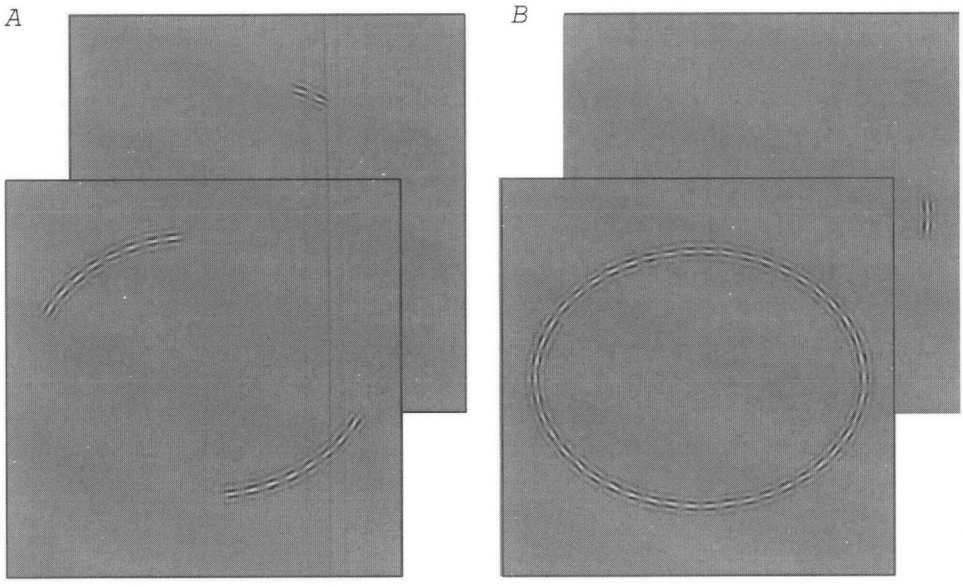

Figure 2. Examples of stimuli used. (A) Stimuli used to test the effect of spatial uncertainty. Two randomly selected ellipse fragments of 8 Gabor patches (foreground) and 2 patches (background). (B) Stimuli used to test temporal summation. Full ellipse (foreground) and 4 patches (two 2-patch fragments) (background). For clarity, the total number of Gabor patches in the ellipse has been reduced, and the size relative to the frame increased (60%).

Target threshold contrast (which ranged from 5 to 40%) was determined by a staircase method, which was shown to converge to 79% correct (Levitt, 1971). With this method, the target contrast is increased by 0.1 log units ($\sim 26\%$) after an erroneous response, and is decreased by the same amount after 3 consecutive correct responses. The number of contrast reversals (from increased to decreased or vice versa) within each block was recorded, and the block was terminated after 8 such reversals. The threshold contrast of a block was the geometric average of the last 6 reversals; the first two were ignored. The threshold results of 4–8 blocks were averaged to compute the mean threshold and standard error of the mean (SE), which were plotted in the figures. In all experiments, observers were instructed to maintain their fixation at the center of the screen and not to move their eyes.

2.1.4. Observers. Two observers GH and YB (one of the authors) participated in the experiments. GH was naive as to the purpose of the experiments, and was paid in return. Both observers had normal or corrected-to-normal vision.

2.2. Results

2.2.1. Spatial uncertainty. Models based on SD theory (Pelli, 1985) predict that spatial uncertainty will affect contrast threshold, since such uncertainty forces the observer to monitor more irrelevant channels with independent noise, and thus

degrades the observer's performance. The effect of spatial uncertainty on contrast summation was tested by repeating previous summation experiments (see Bonneh and Sagi, 1998a), but with randomized target positioning.

Stimuli: Stimuli consisted of two fragments of an elliptic configuration of Gabor patches (see *Methods*), which were randomly positioned between trials, but with 180 deg between them in each trial. An example of the stimuli used is presented in Fig. 2A.

Results: Contrast thresholds (relative to the threshold of a full 73-patch smooth ellipse) were plotted as a function of the number of patches on a log–log scale, for both the uncertainty condition (new data) and the certainty condition (data taken from Bonneh and Sagi, 1998a) and for two observers (Fig. 3). The thresholds for the 73 patches were essentially identical under the two conditions, and thus, were used for normalization. None of the data points for patch number larger than 4 showed significant difference (t-test). In the 2-patch condition for observer GH, uncertainty slightly elevated the relative threshold (0.1 log units). Similar results were obtained for summation along one ellipse-fragment that was randomly positioned.

The weak spatial uncertainty effect is inconsistent with a model based on PS between independent channels using SD, assuming observer's control over the set of monitored channels (Tyler, 1997b). However, the results are compatible with a model based on correlated (or global) noise between detectors, where in absence of interactions (non-collinear elements), performance remains basically flat with an increasing number of targets.

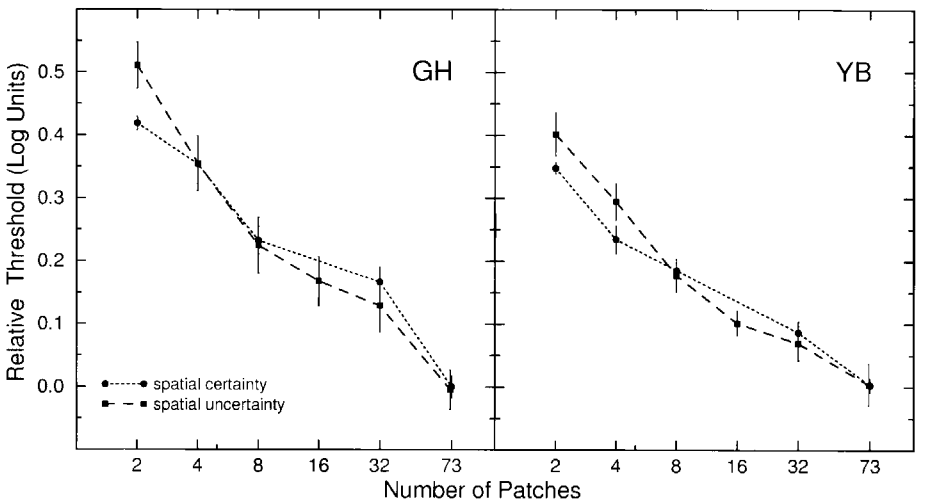

Figure 3. The effect of spatial uncertainty on contrast detection threshold and contrast summation. Detection threshold (relative to the threshold of a 73-patch smooth ellipse) is plotted as a function of the number of patches on a log–log scale for two conditions: spatial uncertainty where the position of the patches is randomized and spatial certainty where it is fixed. Each datum point of the uncertainty data is based on 5–6 measurements. Error bars indicate ± 1 SE. Observers are GH (left) and YB (right). Spatial-certainty data reported from Bonneh and Sagi (1998a).

2.2.2. Temporal summation. In order to further constrain the model, the amount of temporal integration in displays of multiple elements was tested. The data thus obtained, could clarify the effect of probability summation over time (Watson, 1978), and constrain the dynamics of our proposed lateral interaction network.

Stimuli: The stimuli consisted of two fragments of an elliptic arrangement of Gabor patches from the two sides of the horizontal meridian (Fig. 2B), as described in Methods, with a fragment sizes of two patches, 16 patches and a full 73-patch ellipse. The stimuli were all tested for contrast detection threshold with varied presentation time. Each block of trials tested one configuration and presentation time; block order was randomized within a session.

Results: When the contrast thresholds were plotted as a function of presentation time on a log–log scale similar and parallel curves for the different fragment sizes were obtained (Fig. 4). These duration curves support a model based on a combination of linear 'physiological' integration and probability summation over time. For short duration times the threshold curves show a strong improvement (initial exponents > 0.5 ($q < 2$)), which later becomes flatter (exponents < 0.33 ($q > 3$)).

2.2.3. Pedestal effects. When the contrast threshold of a target is measured in the presence of an identical pattern, which is referred to as pedestal (i.e. one frame in a 2AFC paradigm presents the pedestal alone and the other frame presents the target superimposed on the pedestal), the results depend on the contrast of the pedestal. For increasing pedestal contrasts, thresholds typically decrease first, reach a minimum, and then increase again, forming a 'dipper' shaped curve (Nachmias

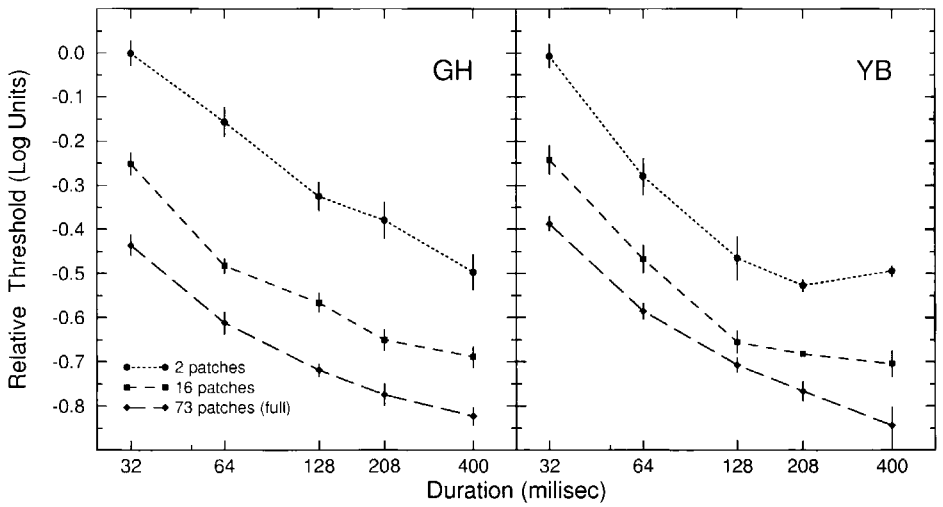

Figure 4. The effect of presentation time on the detection threshold and contrast summation. The detection threshold is plotted as a function of presentation time on a log–log scale relative to the threshold for 2 patches at 32 ms. Each datum point is based on 4–5 measurements. Error bars indicate ± 1 SE. Each panel depicts the results obtained with one observer.

and Sansbury, 1974; Zenger and Sagi, 1996). The facilitation portion of this curve can be accounted for by assuming a threshold or an accelerating transducer function with a similar effect (Nachmias and Sansbury, 1974). Thus, when the pedestal is below threshold, it has no effect on the response to the no-target display, but in the target display it adds its contrast to the target and produces facilitation. This facilitation is maximal for near threshold pedestal. An alternative explanation which does not assume a threshold is based on the uncertainty model (Pelli, 1985) in which facilitation is produced by reducing uncertainty (the relevant channels are stimulated by the pedestal, while the irrelevant ones are not). This model predicts a reduction in pedestal facilitation when the number of elements in a multi-element stimuli is increased, since there is less uncertainty (even without pedestal) when more channels are relevant (see 'model section'). In our model, a threshold was motivated or avoided by testing the effect of the number of elements in a multi-element stimuli on the amount of facilitation by the pedestal.

Stimuli: The stimuli consisted of fragments of an elliptic arrangement of Gabor patches that made a smooth contour around fixation, as in the temporal summation experiments. Detection of the stimuli was tested for two conditions: full 73-patch ellipse and 4 patches in two fragments (2 patches each) from the two sides of the horizontal meridian. The pedestal, which was identical to the target except for having a fixed contrast, appeared in both the 2AFC displays. Pedestal contrast varied from 0 (absolute threshold) to 30%, but was fixed within a block, and ordered from low to high between blocks.

Results: The resulting contrast thresholds were plotted as a function of the pedestal contrast for the two conditions, relative to the detection threshold (pedestal contrast 0) of each condition (Fig. 5). For observer YB the dipper effect (enhance-

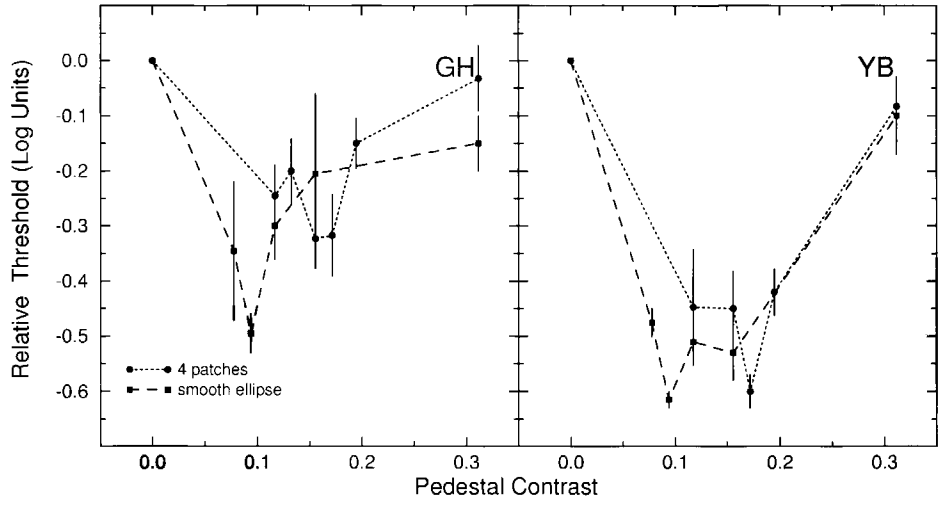

Figure 5. The dipper effect for 73 patches (full ellipse) and 4 patch configuration. Detection threshold is plotted as a function of pedestal contrast for the two conditions. Each datum point is based on 3–4 measurements. Error bars indicate ± 1 SE. Observers are GH (left) and YB (right).

ment relative to the threshold) was 0.6 log units in both conditions and for observer GH, the 4-patch condition yielded a smaller dip.

A strong dipper function was observed; the dipper effect for many patches was identical to or greater than that measured for fewer patches. This is inconsistent with the uncertainty model (Pelli, 1985), where the relative amount of uncertainty decreases with increasing number of targets (i.e. the model predicts facilitation magnitudes in the opposite direction, see 'pedestal effects' in the 'model' section), and supports the existence of a threshold. For both observers, the dipper maxima for the two conditions differed by a factor of 2, as expected with threshold changes due to increased number of patches. The reduced dipper effect for GH with 4 patches was consistent with the narrower dipper observed for the 73 patch ellipse, and probably reflects a lower threshold for the inhibitory 'gain control' process (Zenger and Sagi, 1996).

3. LATERAL SUMMATION MODEL

The Lateral Summation Model presented here is minimal, as we attempted to utilize the simplest set of assumptions which is consistent with both psychophysics and neurophysiology. The model consists of two stages: the network, which implements lateral interactions that result in a deterministic output, and the decision stage, which handles global noise by probability summation over time and global threshold mechanisms. When the model is applied to experimental data obtained by using low contrast stimuli (and thus implying weak responses) response linearity is assumed, except for a threshold (at the decision stage) and negligible inhibitory processes (Adini *et al.*, 1997).

For modeling the network stage, a set of N detectors arranged on a ring structure is assumed ($N = 72$ in all the simulations), one for each possible target element in the display (Bonneh and Sagi, 1998a), as illustrated in Fig. 6 (the difference between the 72 patches used here and the 73 patches used experimentally is technical and insignificant). Each detector is activated, in proportion with its input contrast, by the presence of a target element within its receptive field, and it is assumed that there is no overlap between target elements or receptive fields (i.e. the spacing between elements is large enough). Non-optimal detectors (e.g. tuned to other orientations or spatial frequencies) and the inhibition between detectors, are assumed to be negligible. (These assumptions are clearly invalid for supra-threshold stimuli, thus, this model is applicable only for low contrast stimuli.) The various detectors interact by quasi-local interactions, which decay exponentially with distance and are orientation dependent, so that maximal connectivity weights are made between detectors corresponding to collinear elements and minimal connection weights between detectors that correspond to orthogonal elements. Noise is assumed to be global and to affect all the detectors in the same way (this could result from either correlated or negligible independent noise relative to the noise at later decision stages). Network output is followed by a threshold before being passed to the

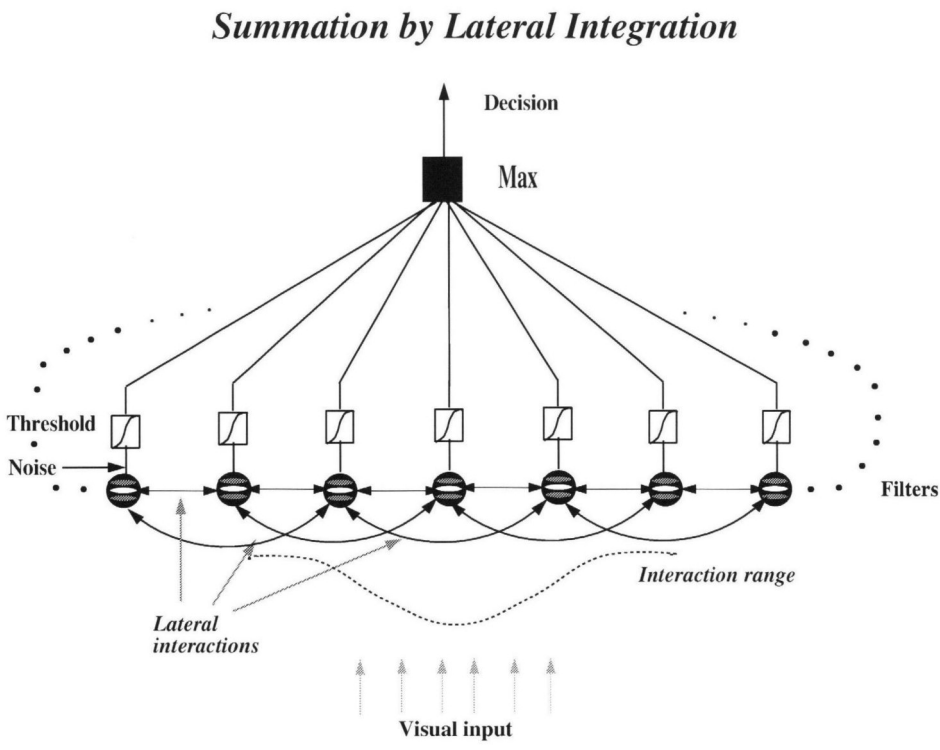

Figure 6. Schematic illustration of the Lateral Summation Model. Collinear orientation selective filters interact through excitatory connections, which decay exponentially with distance. These filters have correlated noise and are followed by a local response threshold. The maximal local activity is then used for decision.

decision mechanism. Thresholds within the network are assumed to be relatively low (set to zero).

The 2AFC performance is computed by comparing the maximal activation which occurs within the detectors, during the signal and the noise frames, incorporating probability summation over time. If the activation during neither frame reaches the network threshold, responses are selected randomly with a probability of 50%. If the maximal activation in only the signal or the noise frame reaches the threshold, then that frame is selected. If the activation in both frames reaches the threshold, the frame with the greater response is selected.

3.1. Computational methods

The activation of the detectors corresponds to the firing rates of neural populations (Amit, 1989; Abbott, 1991; Hertz *et al.*, 1991), and thus obeys the standard equation

$$\tau \frac{\mathrm{d}x_i}{\mathrm{d}t} = -x_i + I_i + \sum_j W_{ij} x_j, \tag{1}$$

where x_i is the activation of detector i and $I_i \geqslant 0$ is the sensory input (proportional to the element's contrast, C), and τ is the time constant for integration and decay of glutaminergic responses (of about 5–10 ms) (Abbott, 1991; Treves, 1992, 1993).

$$W_{ij} = \frac{W_0}{\rho} \exp\left(- \frac{|i - j|}{\rho} \right), \tag{2}$$

describes the lateral connections between detectors, where ρ is a length-scale that characterizes the decay in connectivity with spacing, in units of the shortest inter-element spacing (of 3 times the wave-length of the Gabor elements) as shown in Fig. 2); in the simulations the spatial scale of the interaction was fixed at a value of $\rho = 3$). Due to the first term on the right hand side of equation (1), the pattern of activation converges exponentially to its equilibrium

$$x_i = \sum_j W_{ij} x_j + I_i, \tag{3}$$

if the strength of the lateral connection is bounded by

$$\int \frac{W_0}{\rho} \exp\left(- \frac{x}{\rho} \right) \mathrm{d}x < 1. \tag{4}$$

For the continuous case, the marginal value for the recurrency is $W_0 = 1$. For the discrete case, which was used in our simulation, the integral in equation (4) is replaced with a power series, which results in a marginal value of $W_0 = 0.6$. In the absence of sensory input ($I_i = 0$), the equilibrium solution of the system is $x_i = 0$.

Proximity is modeled by varying the set of units that receive input (e.g. $I_i = 0$ for every other (alternating) unit, corresponds to a spatial separation between the directly activated detectors that is twice as large, than when consecutive detectors are activated).

Network response to a stimulus with n targets, is modeled by numerically solving equations (1) and (2), with $I_i = C$ for $1 \leqslant i \leqslant n$, and $I_i = 0$ for $i > n$ (for non-proximal elements, $I_i = C$ at activated units, and zero otherwise, as explained above), using Euler integration with a time step $\mathrm{d}t = 0.05\tau$.

Equations (1) and (2) provide the deterministic response of the detectors to the visual signal. The maximum of those responses was used to estimate the probability density of the response, when variability is introduced in form of global noise (correlated across detectors), by assuming that at every time window the actual response is distributed as a Gaussian variable with variance σ^2 around the deterministic trajectory of the units. The response in absence of the signal is a Gaussian variable with variance σ^2, which is centered around zero activation.

The interval of stimulus duration was segmented in temporal windows ($T = 20$ Euler iteration steps, i.e. $T = \tau$). If $a_k(C) = a(C, t_k)$ denotes the maximum deterministic activation in the t_k time window, the 2AFC response probability, as a

function of contrast C and temporal duration $K\tau$, can be computed (see Appendix) as:

$$P(C, K) = \int_{\theta}^{\infty} \frac{\mathrm{d}}{\mathrm{d}x}\left[\Pi_{k=1}^{K}\phi(x, a_k(C))\right][\phi(x, 0)]^K \,\mathrm{d}x + \frac{1}{2}\left[\Pi_{k=1}^{K}\phi(\theta, a_k(C))\right][\phi(\theta, 0)]^K, \quad (5)$$

where $\phi(x, a) = \int_{-\infty}^{x} 1/(\sqrt{2\pi\sigma^2})\exp[-(y - a)^2/(2\sigma^2)]\,\mathrm{d}y$ is the cumulative Gaussian integral, K is the total number of time windows, and θ is the threshold (in all the computations reported $\theta = 1$ and $\sigma = 0.4$). The second term of equation (4) represents the probability that neither the signal nor the noise reached threshold during the K time windows, while the first term corresponds to the probability that a signal larger than the threshold is also larger than the noise sample. The multiplication ($\Pi_{k=1}^{K}$) of the probability distributions reflects a form of probability summation over time (Watson, 1978).

For various spatial configurations (patterns of I_i) and temporal durations (K), thresholds were computed by solving numerically (the system of equations (1), (2) and (5)) for the value of contrast C that preserves performance at a level of 80%.

3.2. Simulation results

3.2.1. Spatial summation. The dependency of the threshold on the number of elements (spatial summation) was tested for a collinear configuration in two spacing conditions, according to the experimental manipulation used by Bonneh and Sagi (1998a). The number of elements in the display was increased from 2 to 72 with either (i) fixed-distance spacing between the elements; or (ii) equal spacing among the elements, which divided the ring into equal arcs. The model was tested using $W_0 = 0.4$, $\rho = 3$ and $T = 20\,\mathrm{d}t = \tau$ and a temporal duration of 200 iterations (i.e. 10τ).

The results are shown in Fig. 7 right side, and reproduce the trends of the psychophysical data obtained experimentally in Bonneh and Sagi (1998a); Fig. 7 left side, for both spacing conditions. For the fixed-spacing condition an improvement with an increased number of elements occurred that was approximately power-law with an exponent of $q \approx 4$ (the value of the exponent depends on the strength of the lateral connectivity which was chosen as $W_0 = 0.4$). This observed summation behavior is due to the excitatory lateral interactions between the detectors that perform a type of weighted lateral summation, with effective weights that decay with distance.

For the equal-spacing condition (proximity increasing with the number of elements) virtually no improvement was observed when the distance between the elements was large (corresponding to $n < 8$). In the equal-spacing condition, the improvement took place only when the inter-element distance became compatible with the length-scale (ρ) of lateral interaction of detectors in the network. Note that

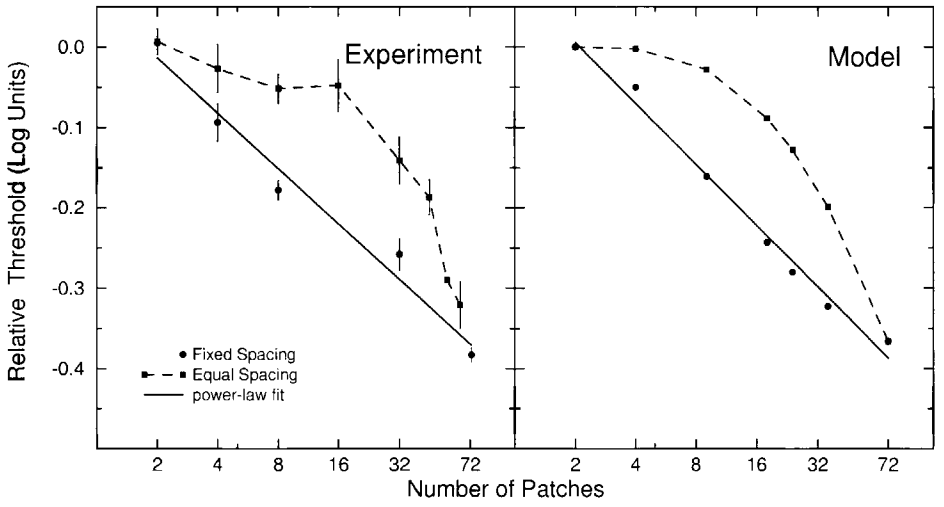

Figure 7. The effect of proximity on contrast detection. Model results (right) are compared with psychophysical data (left) which are the average of two observers from Bonneh and Sagi (1998a), re-plotted from Fig. 1. Detection threshold (relative to the threshold of 2 patches) is plotted as a function of the number of patches on a log–log scale for the two spacing conditions (*equal* (decreasing) and *fixed* (3λ) spacing, as in Fig. 1). The solid curves are power-law fits with exponents of $-1/4.3$ (Experimental) and $-1/4.0$ (Model).

that the stimuli displayed in the two conditions are identical at the extreme points, $n = 2$, and $n = 72$.

3.2.2. Temporal summation. The dependency of the threshold on stimulus duration (temporal summation) was tested for collinear configurations of 2, 16 and 72 patches (arranged on a ring), by manipulating the number of time steps where the network received input $I_i = C$; the simulations were continued for an additional of 60 iterations after the input is cleared (see Fig. 8). Other simulation parameters were identical to the simulations for spatial summation (fixed 3λ spacing condition) and corresponded to these used in the psychophysical experiment of temporal summation assuming 1 ms equivalent to 2 Euler iteration steps (for $\tau = 10$ ms, $dt = 0.05\tau = 0.5$ ms), and covering the 30–200 ms time range (see Section 2).

The threshold duration curves generated by the model were similar to those observed in the experimental data. Both were almost parallel lines, with slopes (on a linear–linear scale) that were larger at the beginning (approximately 0.6) and decreased to approximately 0.33 towards the end. The higher slopes at short durations are due to the local and lateral integration, while the flatter slopes at the end are due to the probability summation over time, which dominates performance when the channel responses, $x(t)$ reach their asymptotic activation. In absence of probability summation over time, the thresholds would not continue to decrease, but instead would reach a finite asymptotic value. In the model the spatial summation increases slightly as a function of duration (the difference between 2 and 72 patches

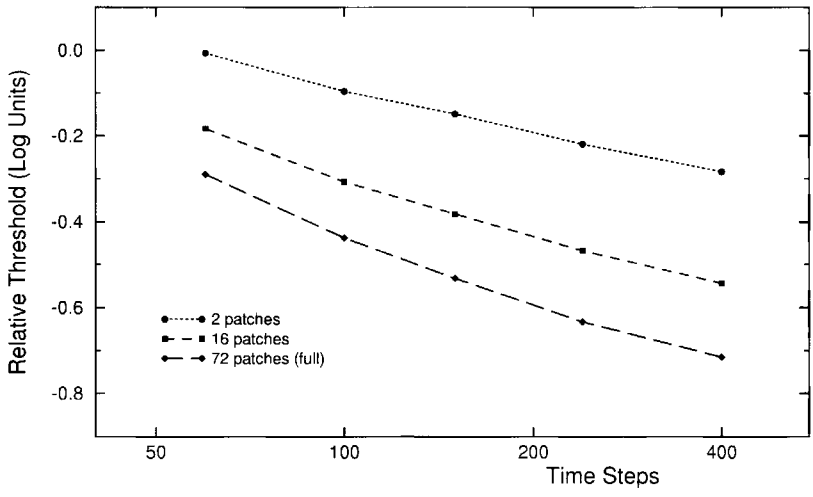

Figure 8. Temporal summation for collinear elements on a ring. Threshold as a function of stimulus duration (iterations) is plotted for three spatial patterns ($n = 2, 16, 72$), relative to the threshold for 2 patches at the shortest duration.

is larger for 400 than for 60 time steps); an increase which does not appear in the psychophysical data, but may reflect the lack of within-channel temporal integration in the model.

3.2.3. Uncertainty effects. The model was designed so that spatial uncertainty effects would not occur (see experiments in the previous section). The absence of spatial uncertainty effects was assured in the model, by assuming that decisions are based on the maximal active unit and that noise is correlated (or global). As a result, the number of spatial channels monitored has no effect on performance, since the maximal response is not influenced by global noise. In the temporal domain, the model uses a scheme based on probability summation over time, which can, in principle, lead to a decrement in detectability for short stimuli with unknown onset time. Nevertheless, due to the relatively high-threshold, the effect of temporal uncertainty is also negligible, in our model. We find that embedding the signal interval within another interval that is 16-fold larger leaves the threshold virtually unchanged. A model based on signal-detection, only (i.e. without a threshold) would have yielded a significant deterioration in performance as the number of noise windows increased.

3.2.4. Pedestal effects. Facilitation as a function of pedestal contrast was tested in the model by modifying equation (4), so that the noise distribution $(\phi(x, 0)^k)$ was replaced by the pedestal distribution with mean C $(\phi(x, C)^k)$ and the signal was scaled to $C + \delta C$. The new threshold, δC, is then computed as a function of the pedestal contrast C, such that performance is preserved at 80%.

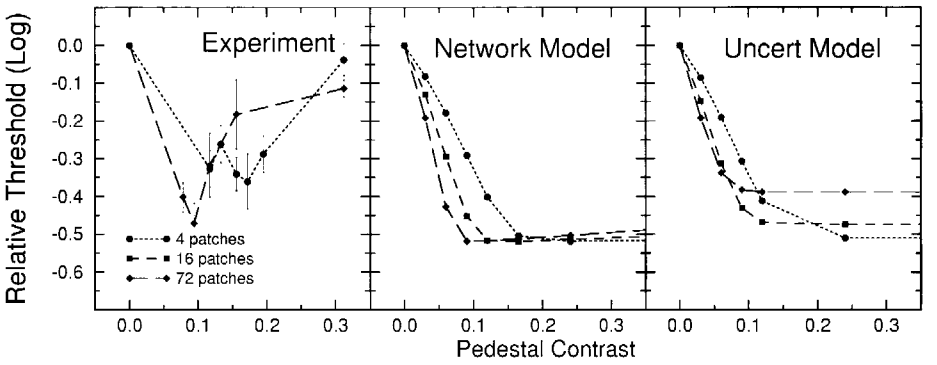

Figure 9. Pedestal facilitation effects for the Lateral Summation Model, the uncertainty model (Pelli, 1985), and experimental data. Left panel — dipper curves for 4 and 72 patch configurations, two observers average (see Section 2). Middle panel — Lateral Summation Model predictions for 4, 16 and 72 patches. Right panel — predictions of the uncertainty model with $M = 1000$. Results are displayed relative to the threshold (zero pedestal) for each configuration in log units, X-axis denotes pedestal contrast.

The pedestal effects predicted by our model and by the uncertainty model (Pelli, 1985) (for $M = 1000$ channels), and those obtained experimentally, are depicted in Fig. 9. The 'dipper' curves were computed for configurations of 4, 16 and 72 patches, using parameters identical to those used for the spatial-summation, fixed-spacing simulation. The computed curves of the model predict only the first part of the dipper curve (i.e. the facilitation at low contrasts), because our model does not include inhibition and thus is not applicable to high contrasts. The facilitation predicted by our model is independent of the number of elements, due to the threshold mechanism used; the pedestal brings both the signal and the noise closer to the threshold, diminishing the fraction of guesses. The magnitude of the facilitation effect is independent of the number of elements since the network serves only as a spatio-temporal filter.

The psychophysical data show more or equal facilitation for the 72 patch configurations than for the 4 patches (with individual differences across observers). As previously explained, this discrepancy between our model and the data could be accounted for by including a lower threshold for the inhibitory 'gain control' process (see Section 2). Nevertheless, the predicted facilitation magnitude of our model (larger or equal for increasing number of targets), as well as the relative pedestal values for the maximal facilitation, are close to the pattern found in the experimental data.

The uncertainty model, which is based on signal detection, has also been shown to produce pedestal facilitation curves (Pelli, 1985), despite the fact that it does not include a threshold mechanism. For this model, facilitation occurs because at weak contrast, the signal is masked by the high response of the many noise channels and due to the fact that this masking effect decreases when the pedestal is added. However, according to this mechanism, the magnitude of the effect should decrease

with the number of target elements; for a fixed number of channels M, increasing the number of target elements leads to a decrease in the relative uncertainty. When the pedestal facilitation was computed, according to the uncertainty model with $M = 1000$ total channels, the maximal facilitation was 0.15 log units less for the 72 element display than for the 4 element display (total facilitation was 0.4 log units) which is inconsistent with, and actually in the opposite direction from that obtained in the experimental data (Fig. 9). Also, the initial slopes of the dipper curves are more similar in the uncertainty model prediction then in the experimental data. With large M values facilitation becomes practically independent of the number of target elements and slope differences increase; however, increasing M has the result of reducing effective summation ($q \approx 5$ with $M = 30000$). An inhibitory process operating at contrast threshold and above, may provide some cure to this problem by having a stronger effect on the 4 element configuration, however, the initial slopes, obtained at low pedestal contrasts, are not expected to be much affected by such an inhibitory process. More detailed measurements are required to estimate these initial slopes and their dependence on the number of targets.

3.3. Further predictions

According to our model, the summation exponent, q, depends on the strength of the lateral connections W_0 and on the spacing between the elements. Proximity effects were discussed in the 'spatial summation' section of the simulation results. In our previously reported results (Bonneh and Sagi, 1998a), and in the current experiments, the inter-element distance was always at least 3 times the spatial scale (λ) of the Gabor filters. By selecting such an inter-element distance, overlap between patches was avoided and multiple-patch integration within standard receptive fields ($\sigma = \lambda$ of a Gabor modeled receptive-field) was prevented, which led to exponents $q \geqslant 4$. A possible prediction is that an exponent $q < 4$ (which corresponds to a stronger summation) should be found if the inter-element distance is reduced to 2.5λ. Since, in the model, the strength of lateral connectivity between detectors is a function of their spacing relative to the interaction scale ρ, a decrease in the shorter inter-element spacing can be simulated by increasing the interaction scale ρ (in the exponent of equation (2), but not in its normalization); an increase in the relative scale of the interaction is equivalent, according to equation (2), to a decrease in the inter-element spacing. However, this prediction should be tested by taking into account (or by avoiding) the linear integration of multiple elements within receptive fields and the linear summation of the stimulus itself (in case of overlap).

4. DISCUSSION

Threshold detection curves obtained in displays with increasing stimulus size were thought to support a model of detection based on probability summation (Sachs

et al., 1971; Robson and Graham, 1981; Pelli, 1985). Thus, detectors were thought to operate independently of each other, and the response to be based on the maximal activation within the set of detectors. Accordingly, the improvement in performance would not be the outcome of spatial integration, but only a result of an increasing probability of detection, which occurs with more targets (if independent noise is assumed). However, the exponents that characterize threshold curves, depend critically on the spatial relationships between the elements (Bonneh and Sagi, 1998a), which contradicts a scheme based on independent detection.

A possible alternative explains the critical proximity range and collinearity constraints with local filters that integrate multiple elements within their receptive fields. Thus, the weak summation observed beyond the critical range would be due to probability summation (e.g. with very high uncertainty (Pelli, 1985)). However, this scheme cannot account for the fourth-root summation observed for proximal and collinear elements (as demonstrated in Fig. 1 for an elongated Gabor filter), because whatever local mechanism is used, the long-range integration beyond the size of the largest mechanism is based on repeated instances of this mechanism combined with the limited probability-summation. Explanation of the long-range integration (which spans a substantial part of a curved contour) with feed-forward mechanisms would require a scheme with a large number of curve detectors for every position and size. Such a scheme has been recently proposed for the linear-summation of orientation information observed in concentric, random-dot Glass patterns (Wilson *et al.*, 1997).

A natural alternative explanation for the improvement in detection observed with increased number of elements is a mechanism based on lateral integration in the cortex. The critical point for such a mechanism is whether the detection curves will reproduce the experimental patterns characterized by power-laws with exponents between 3–4 (Robson and Graham, 1981; Bonneh and Sagi, 1998a). A linear integration scheme would produce either an exponent of 1 (if global noise is assumed) or of 2 (if local independent noise, which is integrated with the signal, is assumed).

Neuroanatomical and the neurophysiological data indicate that cells with similar response properties are interconnected. We propose that this network of lateral connectivity (whose density decays with distance) is the basis for the physiological integration that results in power-law improvements in detection when the elements in the visual display are proximal and collinear. We demonstrated that such a network is able to reproduce a series of findings that are difficult to accommodate within the framework of probability summation. For example, the model explains the dependencies of the threshold curves on the number of elements and stimulus duration, the negligible uncertainty effects, and the proximity and pedestal facilitation effects.

A parameter that strongly affects the summation exponents in the model is the strength of the excitatory lateral connections, W_0. We found that $W_0 = 0.4$ provides the best fit for summation curves, both the spatial and the temporal. Lower values of W_0 result in weak lateral interactions and reduce the spatial summation exponent

to values less than 1/4. Higher W_0 values are likely to produce a state of unbounded activation. In our model, $W_0 = 0.6$ is a marginal value, beyond which the time constant of decay (or integration) becomes infinite (thus activation does not decay anymore). For W_0 values between 0 and 0.6, the passive decay time constant of the neural detectors is amplified by a factor of $0.6/(0.6 - W_0)$. Thus, for $W_0 = 0.4$ the decay constant is multiplied by a factor of three. This is consistent with the canonical micro-circuit scheme, recently proposed by Douglas *et al.* (1995), in which recurrent excitation amplifies neuronal responses to afferent input in the visual system.

An emerging property of the model is a dissociation between the summation exponents, which depend on the deterministic network stage, and the slopes of the psychometric functions which depend on the system noise. Previous models made strong predictions about the relations between summation curve exponents and psychometric functions (Quick, 1974; Robson and Graham, 1981; Tyler, 1997a). Our psychophysical data do not suggest such a clear relation, since similar slopes were obtained regardless of the number of elements and configuration (Bonneh and Sagi, 1998a).

This study was limited to elucidation of the mechanism for subthreshold integration. The physiological and psychophysical data support, in addition, the existence of lateral inhibitory connections. Such connections were not included in the model, since experimental (Cannon and Fullenkamp, 1991; Grinvald *et al.*, 1994; Polat and Norcia, 1996; Zenger and Sagi, 1996; Bonneh and Sagi, 1998b, 1999) and computational (Stemmler *et al.*, 1995) studies indicate that while inhibition dominates lateral interactions at large contrast levels, facilitation dominates at weak sub-threshold levels.

Inclusion of other factors into the model presented here, which are essential for an adequate elucidation of the mechanisms of visual detection, should further refine its fit to the data. Such factors include integration due to the fan-in, feed-forward projections, feedback from higher visual areas, and more complex noise models. For example, local independent noise could be taken into account in combination with global noise as could the dependence of noise variance on the strength of the signal.

Acknowledgement

We thank Yael Adini, Yasuto Tanaka and Uri Polat for helpful discussions and Barbara Schick for reviewing the manuscript. This work was supported by the Basic Research Foundation administered by the Israel Academy of Sciences and Humanities.

REFERENCES

Abbott, L. F. (1991). Realistic synaptic inputs for model neural networks, *Network* **2**, 245–258.

Adini, Y., Sagi, D. and Tsodyks, M. (1997). Excitatory-inhibitory networks in the visual cortex, psychophysical evidence, *Proceedings of the National Academy of Sciences, USA* **94**, 10426–10431.

Amit, D. (1989). *Modelling Brain Functions.* Cambridge University Press, Cambridge.

Bonneh, Y. and Sagi, D. (1998a). Effects of spatial configuration on contrast detection, *Vision Research* **38**, 3541–3553.

Bonneh, Y. and Sagi, D. (1998b). Contrast integration across space, Technical Report GC-DS/98-1, The Weizmann Institute of Science.

Bonneh, Y. and Sagi, D. (1999). Configuration saliency revealed in short duration binocular rivalry, *Vision Research* **39**, 271–281.

Cannon, M. W. and Fullenkamp, S. C. (1991). Spatial interactions in apparent contrast: Inhibitory effects among grating patterns of different spatial frequency, spatial positions and orientations, *Vision Research* **31**, 1985–1998.

Douglas, R. J., Koch, C., Mahowald, M., Martin, K. A. C. and Suarez, H. H. (1995). Recurrent excitation in neocortical circuits, *Science* **269**, 981–985.

Gilbert, C. D. (1992). Horizontal integration and cortical dynamics, *Neuron* **9** (1), 1–13.

Grinvald, A., Lieke, E. E., Frostig, R. D. and Hildesheim, R. (1994). Cortical point-spread function and long range interactions revealed by real-time optical imaging of macaque monkey primary visual cortex, *Journal of Neuroscience* **14**, 2545–2568.

Hertz, A., Krogh, A. and Palmer, R. (1991). *Introduction to Theory of Neural Computation.* Addison-Wesley, Reading, MA.

Howell, E. R. and Hess, R. F. (1978). The functional area for summation to threshold for sinusoidal gratings, *Vision Research* **18**, 369–374.

Kapadia, M. K., Ito, M., Gilbert, C. D. and Westheimer, G. (1995). Improvement of visual sensitivity by changes in local context: parallel studies in human observers and in v1 of alert monkeys, *Neuron* **15**, 843–856.

Knierim, J. J. and Essen, D. C. V. (1992). Neuronal responses to static texture patterns in area-V1 of the alert macaque monkey, *Journal of Neurophysiology* **67**, 961–980.

Kulikowski, J., Abadi, R. and King-Smith, P. (1973). Orientation selectivity of grating and line detectors in human vision, *Vision Research* **13**, 1479–1486.

Legge, G. E. (1978). Space domain properties of a spatial frequency channel in human vision, *Vision Research* **18**, 959–969.

Levitt, H. (1971). Transformed up-down methods in psychoacoustics, *The Journal of the Acoustical Society of America* **49**, 467–477.

Lund, J., Yohioka, T. and Levitt, J. (1993). Comparison of intrinsic connectivity in different areas of cerebral cortex, *Cerebral Cortex* **3**, 148–162.

Malach, R., Amir, Y., Bartfeld, E. and Grinvald, A. (1993). Relationship between intrinsic connections and functional architecture revealed by optical imaging and in vivo targeted biocytin injections in primate visual cortex, *Proceedings of the National Academy of Science, USA* **90**, 10469–10473.

Nachmias, J. and Sansbury, R. V. (1974). Grating contrast: Discrimination may be better than detection, *Vision Research* **14**, 1039–1042.

Palmer, J. (1993). Set size effects in visual search: the effect of attention is independent of the stimulus for simple tasks, *Vision Research* **34**, 1703–1721.

Palmer, J., Ames, C. T. and Lindsey, D. T. (1993). Measuring the effect of attention on simple visual search, *Journal of Experimental Psychology, Human Perception and Performance* **19**, 108–130.

Pelli, D. G. (1985). Uncertainty explains many aspects of visual contrast detection and discrimination, *Journal of the Optical Society of America* **2**, 1508–1532.

Polat, U. and Sagi, D. (1993). Lateral interaction between spatial channels: suppression and facilitation revealed by lateral masking experiments, *Vision Research* **33**, 993–999.

Polat, U. and Norcia, A. M. (1996). Neurophysiological evidence for contrast dependent long range facilitation and suppression in the human visual cortex, *Vision Research* **36**, 2099–2109.

Polat, U. and Tyler, C. W. (1997). What pattern does the eye see best? *Investigative Ophthalmology and Visual Science* **38** (4) (suppl.), S1.

Quick, R. F. (1974). A vector-magnitude model of contrast detection, *Kybernetik* **16**, 65–67.

Robson, J. G. and Graham, N. (1981). Probability summation and regional variation in contrast sensitivity across the visual field, *Vision Research* **21**, 409–418.

Sachs, M. B., Nachmias, J. and Robson, J. G. (1971). Spatial frequency channels in human vision, *Journal of the Optical Society of America* **61**, 1176–1186.

Stemmler, M., Usher, M. and Niebur, E. (1995). Lateral interactions in primary visual cortex: A model bridging physiology and psychophysics, *Science* **269**, 1877–1880.

Treves, A. (1992). Local neocortical processing: a time for recognition, *International Journal of Neural Systems* **3**, 115–119.

Treves, A. (1993). Mean field analysis of neuronal spike dynamics, *Network* **4**, 259–284.

Tyler, C. (1997a). Why we need to pay attention to psychometric function slopes, *Optical Society of America, Technical Digest* **1**, 240–243.

Tyler, C. W. (1997b). Threshold psychophysics, probability summation and the analysis of spatial summation behavior, Prepublished Web paper, URL: http://www.ski.org/CWTyler_lab/CWTyler/PrePublications/ProbSumm/ProbSumm.html.

Watson, A. B. (1978). Probability summation over time, *Vision Research* **19**, 515–522.

Wilson, H. R., Wilkinson, F. and Asaad, W. (1997). Concentric orientation summation in human form vision, *Vision Research* **37**, 2325–2330.

Zenger, B. and Sagi, D. (1996). Isolating excitatory and inhibitory non-linear spatial interactions involved in contrast detection, *Vision Research* **36**, 2497–2513.

APPENDIX: PROBABILITY SUMMATION IN SIGNAL DETECTION MODELS

The predictions of the SD model of probability summation were developed according to the uncertainty model of Pelli (1985). If high uncertainty (the number of channels M, is larger and independent of the number of targets, n) is assumed, the signal and the noise distribution functions (for the maximum response) are computed as:

$$F_N(x, n, M) = \phi^M(x), \tag{A.1}$$

$$F_S(x, n, M) = \phi^n(x - C)\phi(x)^{M-n}, \tag{A.2}$$

where x is the noisy filter response, $\phi(x)$ is the cumulative distribution of responses and C is the contrast of the signal that generates the response.

The probability that a sample chosen from the signal distribution is larger than a sample chosen from the noise distribution can be computed by

$$P(C) = \int_{-\infty}^{\infty} \left[\frac{\mathrm{d}}{\mathrm{d}x} F_S(x, C)\right] F_N(x)\,\mathrm{d}x. \tag{A.3}$$

The upper curve in Fig. A.1 depicts the threshold for detection as a function of n for an uncertainty corresponding to $M = 1000$ channels, assuming the cumulative distribution $\phi(x)$ to be a Gaussian integral. The estimated exponent is $q = 3.8$.

In the absence of uncertainty (i.e. $M = n$), equations (A.1) and (A.2) should be replaced with:

$$F_N(x, n, M) = \phi^n(x), \tag{A.4}$$

$$F_S(x, n, M) = \phi^n(x - C). \tag{A.5}$$

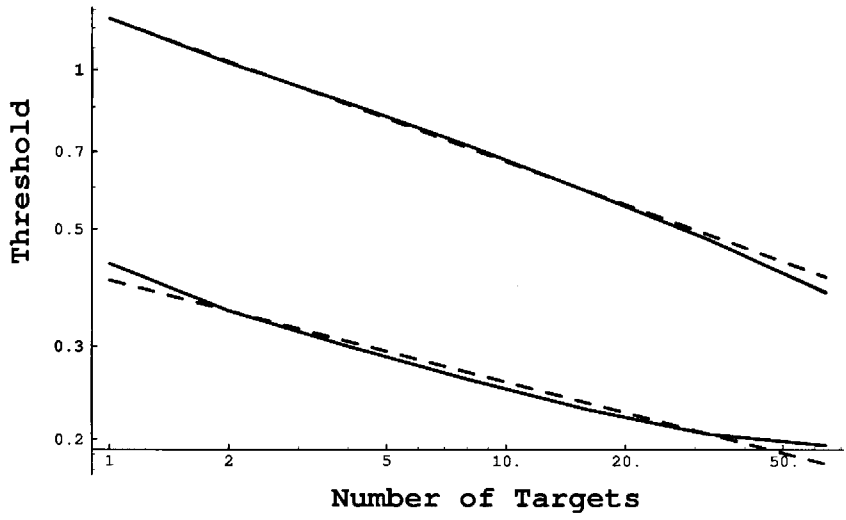

Figure A.1. Summation curves for the signal detection model of probability summation. Upper curve corresponds to an uncertainty of $M = 1000$ channels, which results in $q = 3.8$ (Pelli, 1985). Lower curve corresponds to a model without uncertainty (see Tyler, 1997), which results in $q = 5.2$. The dashed curves are power-law fits, with exponents of $-1/5.2$ and $-1/3.8$ for the upper and lower curves, respectively.

This yields flatter threshold curves (see the lower curve in Fig. A.1). When the processes are identical, the two curves should intersect at $n = 1000$. For $n < 1000$, the model without uncertainty results in superior performance (a lower threshold) and a flatter curve (estimated $q = 5.2$).